Lattice dynamics of random and quasiperiodic heterostructures

Raedt, H. De; Schneider, T.

Published in:
Zeitschrift für Physik. B: Condensed Matter

DOI:
10.1007/BF01312487

Publication date:
1988

Z. Phys. B – Condensed Matter 71, 287–293 (1988)

Condensed Matter
Zeitschrift für Physik B

Lattice dynamics of random and quasiperiodic heterostructures

H. De Raedt * **and T. Schneider**
IBM Research Division, Zürich Research Laboratory, Rüschlikon, Switzerland

Received December 1, 1987

We report on the quantum-mechanical displacement form factor in quasiperiodic and random heterostructures. A one-dimensional treatment is adopted to describe the longitudinal displacement along the growth axis. Elastic properties are assumed to be homogeneous, while the inhomogeneous mass density characterizes the heterostructure. In the low-frequency limit, the peak structure can be attributed to acoustic phonons, whereas for higher frequencies the quasiperiodic and random cases differ markedly. In the quasiperiodic case and constant momentum transfer, resonances separated by gaps occur and their number depends on the resolution in the frequency domain. The random case is dominated by an acoustic resonance becoming broader with increasing frequency.

1. Introduction

In this work, we study the properties of phonons propagating parallel to the growth axis of heterostructures. The ability to produce heterostructures is a revolutionary advance, allowing the growth of systems consisting of layers of material with nanometer spacing. Potential device applications initiated studies of electronic and transport properties, in particular of doped and undoped semiconductor superlattices and quantum-well heterostructures [1]. Much less attention was devoted to random and quasiperiodic heterostructures. Here the layers consisting of building blocks, are grown at random or according to a deterministic rule, exhibiting no periodicity. In analogy to the periodic case, a one-dimensional (1-D) treatment appears to be appropriate to describe properties along the growth axis [1]. Adopting the 1-D description, we study the propagation of longitudinal phonons in random and quasiperiodic heterostructures. Elastic properties are assumed to be homogeneous, while the inhomogeneous mass density characterizes the heterostructure.

In Sect. 2, we sketch the formalism to calculate the integrated density of states, the inverse exponential localization length and the dynamic form factor of the displacements. Here, we also point out the connection to the tight-binding Schrödinger problem for an electron in a random and quasiperiodic potential. In Sect. 3, we present and discuss the numerical results, including the integrated density of states, the inverse exponential localization length and the dynamic form factor. In the quasiperiodic case, we consider two models, differing in the deterministic rule, assigning the mass density M_n of the n-th layer. As seen from Table 1, quasiperiodicity in Model I is obtained from irrational Q-values, while in Model II the mass density is given by the Fibonacci sequence. For comparison, we also treat the periodic counterpart of Model I, with a $Q=1/5$, representing a crude approximant to $Q=(\sqrt{5}-1)/(2\pi)$. Model III refers to the random case.

Our main results include: In the low-frequency limit, the peak structure of the quantum-mechanical zero-temperature displacement form factor can be at-

Table 1. Definition of the models

Model	M_n
I	$M_n=A+B\cos(2\pi Q n)$
II	Fibonacci sequence
III	Random

* Permanent address: Department of Physics of Antwerp, Universiteitsplein 1, B 2610 Wilrijk, Belgium

tributed to acoustic phonons, while for higher frequencies the quasiperiodic and random systems differ drastically. In the quasiperiodic case and constant momentum transfer, resonances separated by gaps occur and their number is limited by the resolution in the frequency domain. The random case is dominated by an acoustic resonance becoming broader with increasing frequency. In comparison with the quasiperiodic Model I, both Fibonacci and random heterostructure are found to have enhanced Debye-Waller factors. Inclusion of inhomogeneous elastic properties and equilibrium spacings of the heterostructure we leave for future studies.

2. Sketch of the formalism

Restricting our study to longitudinal displacements, the discretized equation of motion reads [2]

$$-M_n \omega^2 u_n = f(u_{n+1} + u_{n-1} - 2u_n). \tag{1}$$

M_n denotes mass density, u_n displacement of the n-th layer, ω is the frequency and f the elastic constant, assumed to be homogeneous. For numerical treatments, it is convenient to rewrite (1) in the form [3]

$$R_{n+1} = -1/R_n + 2 - \frac{M_n \omega^2}{f}, \quad R_{n+1} = \frac{u_{n+1}}{u_n} \tag{2}$$

corresponding to a recursion relation. The integrated density of states is then obtained, in terms of node counting, from

$$N(\omega) = \frac{1}{N} \sum_{n=1}^{N} A_n, \quad A_n = \begin{cases} 1 & \text{for } R_n < 0 \\ 0 & \text{otherwise.} \end{cases} \tag{3}$$

The inverse exponential localization length is given by [3]

$$\gamma(\omega) = \frac{1}{N} \sum_{n=1}^{N} \ln |R_n|, \tag{4}$$

where

$$\gamma(\omega) \geqq 0. \tag{5}$$

Rewriting (1) in the form

$$u_{n+1} + u_{n-1} - 2u_n = -\frac{M_n}{f} \omega^2 u_n, \tag{6}$$

the connection to the Schrödinger problem

$$\varphi_{n+1} + \varphi_{n-1} - 2\varphi_n = (V_n - E)\varphi_n \tag{7}$$

for a tightly-bound electron in the presence of a potential V with strength V_n at the n-th site, is obvious. This equation also models the electronic properties of quantum-well superlattices, along the growth axis. For random and δ-correlated V_n's, it corresponds to the 1-D Anderson model [4]. Recently, the quasiperiodic case evoked considerable interest [5, 6]. In fact, quasiperiodicity provides a link to understanding of the crossover between corresponding properties resulting from periodic and random potentials. Periodic potentials lead to continuous spectra (bands) with gaps and extended wave functions, while random and uncorrelated potentials exhibit pure point spectra and exponentially localized wave functions. There is considerable evidence for much richness in the quasiperiodic case. Highly fragmented integrated density of states [5, 6] transition from extended to localized wave functions [7] and algebraic localization can occur [8]. Invoking the equivalence between the equation of motion for lattice dynamics (1), and the Schrödinger problem (7), it is clear that these phenomena will also appear in the lattice-dynamic case. However, there is a crucial difference stemming from the fact that in lattice dynamics, the lowest eigenvalue $\omega = 0$ is fixed and the corresponding displacements u_n are extended. Consequently, the leading term in the integrated density of states $N(\omega)$ can be calculated exactly. The result is [9]

$$\lim_{\omega \to 0} \frac{N(\omega)}{\omega} = \frac{1}{\pi} \left(\frac{\langle M \rangle}{f} \right)^{1/2}, \tag{8}$$

where

$$\langle M \rangle = \frac{1}{N} \sum_{n=1}^{N} M_n. \tag{9}$$

To calculate the dynamic form factor of the displacements,

$$S_{uu}(q, \omega) = \int_{-\infty}^{+\infty} \mathrm{d}t \, \mathrm{e}^{\mathrm{i}\omega t} \langle u(q, t) \, u(-q, 0) \rangle, \tag{10}$$

where

$$u(q, t) = \frac{1}{\sqrt{N}} \sum_{l} \mathrm{e}^{\mathrm{i}ql} u_l(t), \tag{11}$$

we adopt two approaches.

For Model I and its periodic counterpart (Table 1) it is useful to reformulate (1) in terms of the wave number dependent displacement $u(q)$, yielding

$$\left[\frac{A}{f} \omega^2 + 2(1 - \cos q) \right] u(q) - \frac{B\omega^2}{f} (u(q+Q) + u(q-Q)) = 0. \tag{12}$$

Adding integer multiples of Q to q, one obtains from (12) the recursive relation

$$\left[\frac{A}{f}\omega^2+2(1-C_n)\right]u_n-\frac{B\omega^2}{f}(u_{n+1}+u_{n-1})=0, \tag{13}$$

where

$$C_n=\cos(q+nQ), \qquad X_n=u(q+nQ). \tag{14}$$

Thus for fixed q, the problem is reduced to an eigenvalue problem of a tridiagonal matrix, with eigenvalues $\omega_\alpha(q)$ and normalized eigenvectors Y_α, where $-\frac{N}{2}\leqq\alpha\leqq\frac{N}{2}$ and $X_n=\sum_\alpha u_{n\alpha}Y_\alpha$. The quantum-mechanical and zero-temperature expression for the dynamic form factor is then obtained from

$$\tilde{S}_{uu}(q+nQ,\omega)=\sum_\alpha\frac{|u_{n\alpha}(q)|^2}{2\omega_\alpha(q)}\delta(\omega-\omega_\alpha(q)) \tag{15}$$

in terms of

$$S_{uu}(q,\omega)=\sum_n\tilde{S}_{uu}(q+nQ) \tag{16}$$

by reducing the $q+nQ$ to the interval $[-\pi,\pi]$, corresponding to the first Brillouin zone.

In Models II and III, the masses are assigned according to the Fibonacci sequence or at random. Here, one has to treat the equation of motion (1) direct. Adopting free boundary conditions, and introducing the matrices

$$A=\begin{pmatrix}2&-1&0&0&\ddots\\-1&2&-1&0&\ddots\\0&-1&2&-1&\ddots\\\ddots&\ddots&\ddots&\ddots&\ddots\end{pmatrix},$$

$$B=\begin{pmatrix}M_{1/f}&0&\ddots\\0&M_{2/f}&\ddots\\\ddots&\ddots&\ddots\end{pmatrix} \tag{17}$$

the equivalent of (1) reads

$$(B^{-1/2}AB^{-1/2}-\omega^2E)\,Y=0 \tag{18}$$

yielding eigenvalues ω_α ($\alpha=1,\ldots,N$) and eigenvectors $Y_{n\alpha}$. The quantum-mechanical and zero-temperature expression for the displacement dynamic form factor is then

$$S_{uu}(q,\omega)=\sum_\alpha\frac{|X_\alpha(q)|^2}{2\omega_\alpha}\delta(\omega-\omega_\alpha), \tag{19}$$

where

$$X_\alpha(q)=\sqrt{\frac{2}{N+1}}\sum_{l=1}^{N}\sin\pi\frac{q\cdot l}{N+1}X_{e\alpha}, \qquad X=B^{1/2}Y. \tag{20}$$

The numerical results for $S_{uu}(q,\omega)$ are conveniently expressed in terms of the normalized dynamic form factor

$$\hat{S}(q,\omega)=\frac{S_{uu}(q,\omega)}{S_{uu}(q)}, \tag{21}$$

where

$$S_{uu}(q)=\int_0^\infty S_{uu}(q,\omega)\,\mathrm{d}\omega \tag{22}$$

is the static form factor. $S_{uu}(q,\omega)$ and $S_{uu}(q)$ are proportional to the one-phonon coherent inelastic and elastic neutron-scattering cross sections, respectively. $S_{uu}(q)$ also determines the Debye-Waller factor in terms of $W(q)\sim q^2S_{uu}(q)$.

3. Numerical results and discussion

In this section, we present and discuss the numerical results for the integrated density of states (3), the inverse exponential localization length (4) and the dynamic form factor of the displacements.

3.1. *Model I*

With

$$M_n=A+B\cos(2\pi Qn), \tag{23}$$

the equation of motion (1) reads

$$u_{n+1}+u_{n-1}-\frac{B\omega^2}{f}\cos 2\pi Qn\,u_n=\left(\frac{A\omega^2}{f}+2\right)u_n. \tag{24}$$

It is closely related to Harper's equation, extensively studied in the context of Bloch electrons in a magnetic field [10], the transition from extended to exponentially localized states [6, 7], granular superconductors and superconducting networks [11]. Harper's equation reads

$$\varphi_{n+1}\varphi_{n-1}+\alpha\cos(2\pi\beta_n+\theta)\,\varphi_n=E\varphi_n. \tag{25}$$

It is known to exhibit a transition at $\alpha=2$ for $-\pi\leqq\theta\leqq\pi$ and irrational β [6, 7]. If $\alpha>2$, the wave functions are exponentially localized and there is a dense-point spectrum. For $\alpha<2$, the φ_n are extended and the spectrum is continuous. Thus, in the lattice model frequency

$$\alpha=\frac{B\omega_c^2}{f}=2 \tag{26}$$

separates extended and exponentially localized displacements, as well as the occurrence of a continuous and a point spectrum.

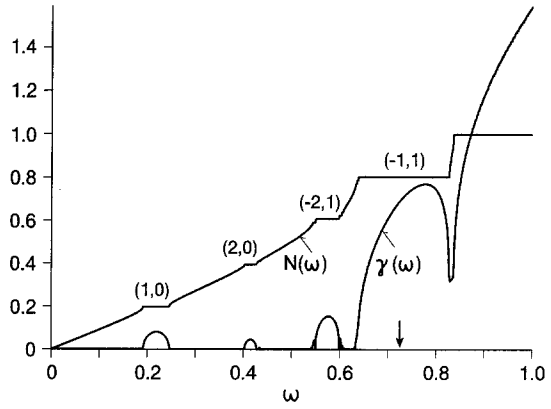

Fig. 1. Integrated density of states $N(\omega)$ and inverse exponential localization length $\gamma(\omega)$ as obtained from iterating (2) for Model I with parameters listed in (27) for $N=10^4$ and $\omega=10^{-3}$. The arrow marks the frequency below which the spectrum is continuous between the gaps, while above, a point spectrum occurs in between the gaps. The gap labeling follows (28)

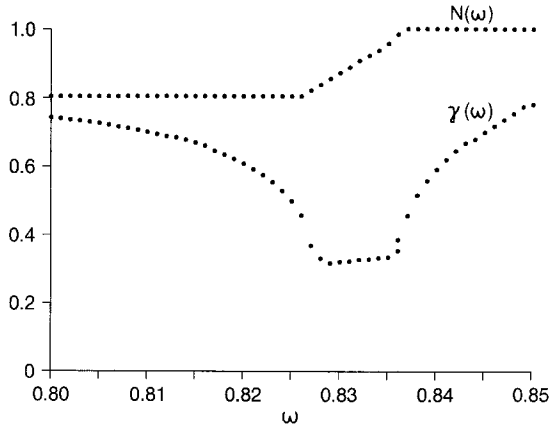

Fig. 2. Blow-up of integrated density of states $N(\omega)$ and inverse exponential localization length $\gamma(\omega)$ depicted in Fig. 1 for ω-values close to the top. $N=2\cdot10^4$ and $\Delta\omega=5\cdot10^{-4}$

Figure 1 shows the integrated density of states $N(\omega)$ and the inverse exponential localization length $\gamma(\omega)$ for Model I with

$$A=2, \quad B=1, \quad f=1/4, \quad Q=\frac{\sqrt{5}-1}{2\pi}. \tag{27}$$

The gaps corresponding to the plateaus can be labeled by two integers, n and m. The integrated density of states below gap n, m is then given by

$$0\leqq N_{n,m}(\omega)=n\frac{Q}{2\pi}+m\leqq 1. \tag{28}$$

The labeling of major gaps is also depicted in Fig. 1. For small ω-values, $N(\omega)$ approaches the expected linear behavior given by (8), but with increasing ω fragmentation becomes more pronounced. It should be kept in mind, however, that beyond the resolution of Fig. 1 there is an infinite number of gaps, with rapidly decreasing width. The major gaps are also signaled by the nonvanishing inverse exponential length $\gamma(\omega)$. For $\omega<\omega_c=1/\sqrt{2}$, the displacements associated with values pertaining to the spectrum are extended. For $\omega>\omega_c$, there is only a small frequency window left, separating gap $(-1, 1)$ and the top. In this window, there are frequencies in the spectrum. They form a point spectrum, and the corresponding displacements are exponentially localized. This behavior is visible in Fig. 1, and clearly seen in Fig. 2, showing a blow-up of this frequency window. In fact $\gamma(\omega)$ remains finite, revealing the exponential localization of the displacements.

To study some implications of this rich excitation spectrum and the localized nature of the displacements, we next consider the behavior of the quantum-mechanical form factor at zero temperature. In doing so, it is instructive to treat a closely related periodic system for comparison. $Q=1/5$ is a crude but reasonable rational approximant to the irrational number $Q=(\sqrt{5}-1)/(2\pi)=0.196726\ldots$. With this choice, M_n (21) becomes periodic, with five particles in the unit cell. As depicted in Fig. 3, there are one acoustic, four optic branches and four gaps. Moreover, on the resolution scale of Fig. 1, the resulting integrated density of states looks very much the same as in the quasiperiodic counterpart. Nevertheless, in the periodic case all displacements are extended, while in the quasiperiodic model exponential localization sets in for $\omega>\omega_c$. The associated dynamic form factor, as calculated from (13), (15) and (16), is depicted in Fig. 4, for 64 ω- and 32 q-channels. The resonance structure is readily traced back to the five phonon branches and their

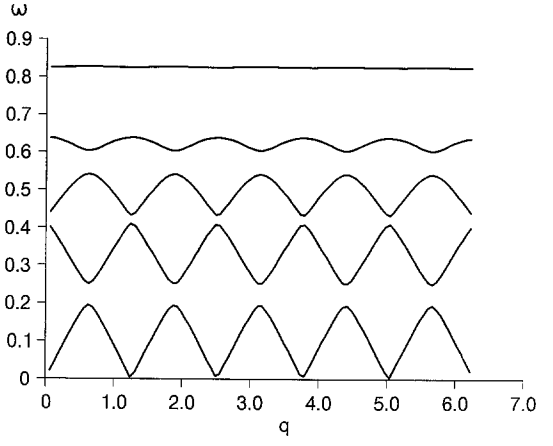

Fig. 3. Phonon-dispersion curves for the periodic version of Model I (23) with $Q=1/5$ and parameters listed in (27)

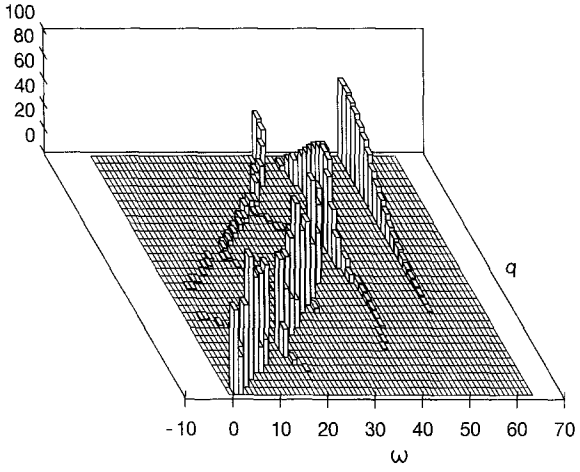

Fig. 4. Dynamic form factor $\hat{S}_{uu}(q, \omega)$ (16) for the periodic Model I (23) for $Q=1/5$ and parameters listed in (27), $q=n\pi/32$, $n=1, \ldots, 32$; $\omega=n/64$, $n=1, \ldots, 64$

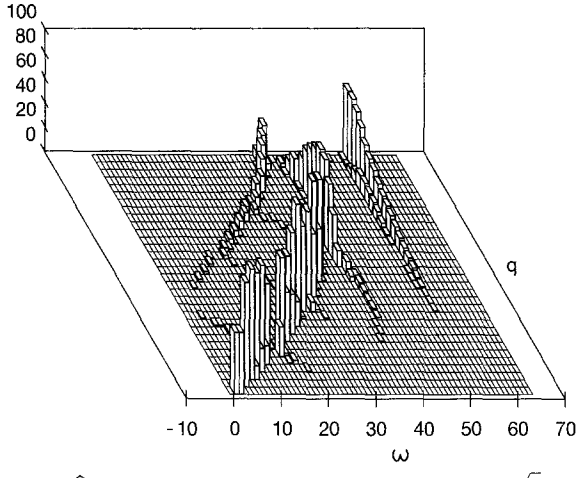

Fig. 5. $\hat{S}_{uu}(q, \omega)$ for the quasiperiodic Model with $Q=(\sqrt{5}-1)/(2\pi)$ and parameters listed in (27) for $N=512$. The grid in q and ω is identical to that in Fig. 4

q-dependence, as shown in Fig. 3. Although all displacements are extended, localization effects are rather pronounced with increasing frequency, because the q-dependence of the resonance structure becomes flat, in agreement with the dispersion laws. The dynamic form factor of the corresponding quasiperiodic model with $Q=(\sqrt{5}-1)/(2\pi)$ is shown in Fig. 5. Comparing these results with Fig. 4, there is no dramatic difference. Clearly, in the quasiperiodic case, in principle, there is an infinite number of branches. Owing to limited resolution, fixed by the width of the channels, only dominating features are seen, well approximated by the periodic counterpart with $Q=1/5$. In fact, the four major gaps are readily seen in Fig. 5, and the q-dependence of the resonance structure becomes flatter with increasing ω. Moreover, the highest q-independent resonance, arising from exponentially localized displacements, does not differ much from the local optic mode in the periodic model.

It is worthwhile noting that, for $A=B=2$, ω_c is not in a gap and the associated displacements are expected to be algebraically localized [5–7]. Exploring this point, we iterated recursion relation (2) for chains up to $N=10^8$ to estimate $\beta_N=\sum_{n=1}^{N} \ln|R_n|/\ln(N)$. Our results revealed strong fluctuations in β_N (even for $N=10^8$) and a pronounced dependence on the initial conditions. The mean value $\langle\beta_N\rangle$ fluctuates between 0.3 and 0.7. Thus, further work is needed to elucidate the nature of localization for ω_c values which are not in a gap.

3.2. *Model II*

In this system, mass M_n is assigned according to the Fibonacci sequence

$$M_n=A+B_n, \tag{29}$$

where

$$\begin{aligned} B_{n+1}&=-2[\theta_n+1/\sigma_G]_I+1 \\ \theta_{n+1}&=[\theta_n+1/\sigma_G]\text{: mod } 1 \\ \sigma_G&=\frac{\sqrt{5}-1}{2}, \quad \theta_0=\sqrt{5}-2, \quad B_0=-1. \end{aligned} \tag{30}$$

A pictorial illustration of the generation of the sequence is given in Table 2. Models of this type have been studied quite extensitvely [5] and even an exact renormalization-group scheme was developed to unravel scaling properties of the integrated density of states and the displacements [9]. Numerical results for the integrated density of states $N(\omega)$ and the inverse exponential localization length $\gamma(\omega)$ are shown

Table 2. Generation of a Fibonacci sequence with F_l elements. F_l denotes the 1-th Fibonacci number, and A corresponds to mass $M_A=1$, while B denotes mass $M_B=3$

l	F_l	Fiobanacci sequence
0		B
1	1	A
2	2	AB
3	3	ABA
4	5	$ABAAB$
5	8	$ABAABABA$
6	13	$ABAABABAABAAB$

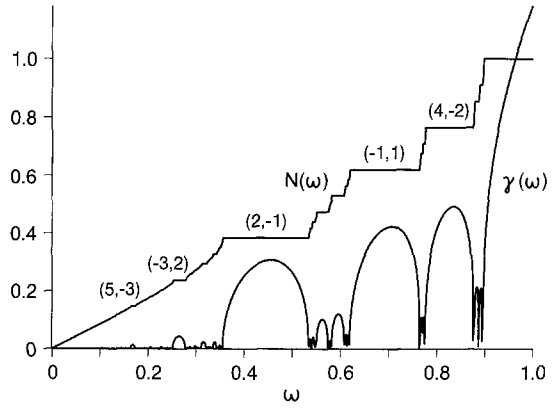

Fig. 6. $N(\omega)$ and $\gamma(\omega)$ for ModelII with masses $M=1$, 3, assigned according to the Fibonacci sequence (Table 2, (28)) for $N=10^4$ and $\Delta\omega=10^{-3}$ as obtained from iterating (2)

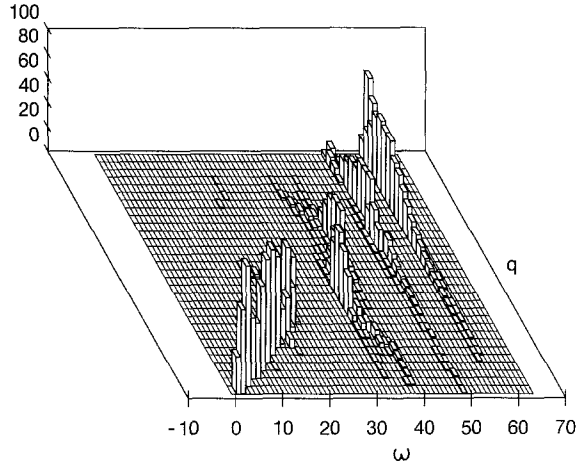

Fig. 7. $\hat{S}_{uu}(q, \omega)$ for Model II, with masses 1, 3 assigned according to the Fibonacci sequence for $N=512$, $q=n\pi/32$, $n=1, \ldots, 32$ and $\omega=n/64$, $n=1, \ldots, 64$

in Fig. 6 for

$$A=2, \quad f=1/4. \tag{31}$$

In the limit $\omega \to 0$ the expected linear frequency dependence (8) is clearly seen, and fragmentation of the spectrum becomes more pronounced with increasing ω. The gaps can again be labeled by two integers n, m, where the integrated density of states below gap n, m is given by

$$0 \leqq N_{n,m}(\omega)=n+m\sigma_a \leqq 1. \tag{32}$$

This labelling is depicted in Fig. 6 for the major gaps. Again, there is an infinite number of gaps, with gradually diminishing width and beyond the resolution scale of Fig. 6. The visible gaps are also signaled by the finite value of the inverse exponential localization length. For the frequencies belonging to the spectrum, one expects algebraic localization.

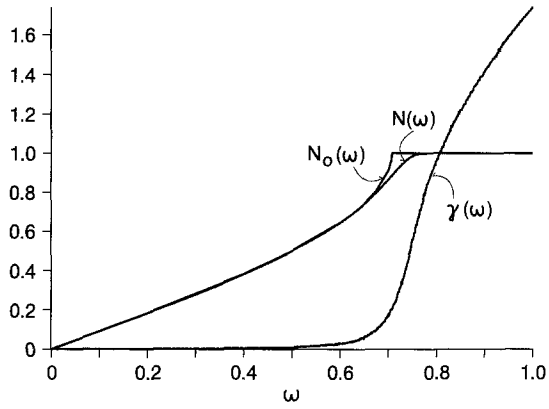

Fig. 8. $N(\omega)$ and $\gamma(\omega)$ for Model III with randomly assigned masses (33) for $N=10^4$ and $\Delta\omega=10^{-3}$. For comparison, we included $N(\omega)$, resulting from the average mass approximation (36)

The dynamic form factor of this model, as calculated with the aid of (18)–(20) for a chain of $N=512$, is shown in Fig. 7. At low frequencies, there is a resonance structure which can be attributed to acoustic phonons, while for higher frequencies nearly q-independent peaks occur only, revealing the localized nature of the displacements with frequencies in between the major gaps (2, −1), (−1, 1) and (4, −2) (Fig. 6). In a larger system allowing increased resolution in the frequency domain, these peaks are expected to split, because new, but narrower gaps will occur (32).

3.3. *Model III*

Finally, we consider the case of randomly assigned masses, where

$$M_n=A+B_n$$

$$P(B_n)=\begin{cases}1/2: & \text{if } -\Delta \leqq \beta_n \leqq \Delta \\ 0: & \text{otherwise.}\end{cases} \tag{33}$$

In this case and for the infinite chain, all displacements are exponentially localized and the spectrum is point. Numerical results for $N(\omega)$ and $\gamma(\omega)$ are shown in Fig. 8, for

$$A=2, \quad \Delta=0.5, \quad f=1/4. \tag{34}$$

In the low-frequency limit, localization is seen to be weak and the frequency dependence of $N(\omega)$ is linear. There are no gaps and at the top the expected Lifshitz tail behavior becomes visible [12]. Here, appreciable exponential localization sets in. The absence of gaps and the nearly continuous behavior differ markedly from the periodic and quasiperiodic (Fig. 5) cases. In fact, not only the low, but also the intermediate frequency regime of $N(\omega)$ are well approximated by an

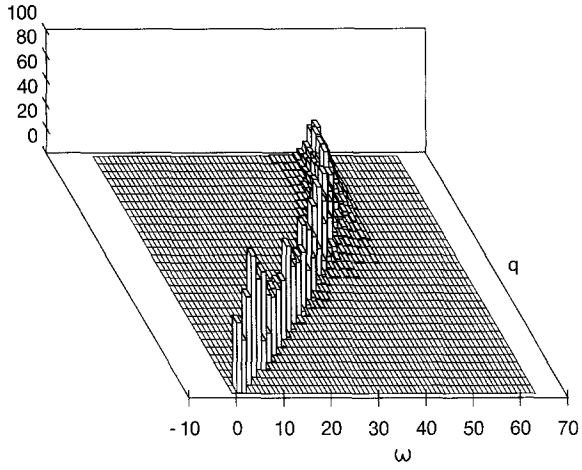

Fig. 9. $\hat{S}_{uu}(q, \omega)$ for Modell III with randomly assigned masses (33) for $N=512$. The grid for q and ω is identical to that in Fig. 7

average mass modes with frequency

$$\omega^2=\frac{2f}{\langle M\rangle}(1-\cos q), \qquad \langle M\rangle=A \tag{35}$$

yielding

$$N_0(\omega)=\frac{2}{\pi}\arcsin\left(\frac{\omega}{2}\left(\frac{\langle M\rangle}{f}\right)^{1/2}\right). \tag{36}$$

This expression leads to the exact low-frequency limit (8). For comparison, $N_0(\omega)$ is included in Fig. 8 and differs from $N(\omega)$ close to the top only, where the Lifschitz tail behavior [12] sets in. Accordingly, we expect the dynamic form factor to be dominated by a resonance with dispersion (35) and richer structure appearing at higher frequencies. The numerical results shown in Fig. 9 fully confirm this expectation.

We thank P. Soerensen and D. Würtz for stimulating discussions. One of us (H.D.R.) thanks the National Science Foundation of Belgium for financial support.

References

1. For a recent review, see Esaki, E.: In: Proceedings of the 17th International Conference of Physics of Semiconductors. Chadi, J.D., Harrison, W.A. (eds.), p. 473. Berlin, Heidelberg, New York: Springer 1985
2. Merlin, R., Bajema, K., Clarke, R., Huang, F.Y., Battacharaya, P.K.: Phys. Rev. Lett. **55**, 1768 (1985)
3. Schneider, T., Würtz, D., Politi, A., Zannetti, M.: Phys. Rev. B **36**, 1789 (1987)
4. Erdös, P., Herndon, R.C.: Adv. Phys. **31**, 65 (1982)
5. Sokoloff, J.B.: Phys. Rep. **126**, 189 (1985)
6. Simon, B.: Adv. Appl. Math. **3**, 463 (1982)
7. Aubry, S., Andre, C.: In: Proc. Isreal Phys. Soc. Kuper, C.G. (ed.), p. 133. Bristol: Hilger 1979
8. Schneider, T., Politi, A., Würtz, D.: Z. Phys. B – Condensed Matter **66**, 469 (1987)
9. Würtz, D., Schneider, T., Politi, A.: (to be published)
10. Hofstadter, D.R.: Phys. Rev. B **14**, 2239 (1976)
11. Pannetier, B., Chaussy, J. Rammel, R.: J. Phys. Lett. **44**, 853 (1983)
12. Politi, A., Schneider, T.: (to be published)

H. De Raedt
Department of Physics
University of Antwerp
Universiteitsplein 1
B-2610 Wilrijk
Belgium

T. Schneider
IBM Research Division
Zürich Research Laboratory
Säumerstrasse 4
CH-8803 Rüschlikon
Switzerland